



# Optics Letters

## Distortion-free multi-element Hypergon wide-angle micro-objective obtained by femtosecond 3D printing

KSENIA WEBER,<sup>1,†</sup>  ZHEN WANG,<sup>1,†</sup> SIMON THIELE,<sup>2</sup> ALOIS HERKOMMER,<sup>2</sup> AND HARALD GIESSEN<sup>1,\*</sup>

<sup>1</sup>4th Physics Institute and Research Center SCoPE, University of Stuttgart, Pfaffenwaldring 57, 70569 Stuttgart, Germany

<sup>2</sup>Institute for Applied Optics and Research Center SCoPE, University of Stuttgart, Pfaffenwaldring 9, 70569 Stuttgart, Germany

\*Corresponding author: h.giessen@pi4.uni-stuttgart.de

Received 11 March 2020; revised 2 April 2020; accepted 5 April 2020; posted 10 April 2020 (Doc. ID 392253); published 12 May 2020

**In this Letter, we present a 3D-printed complex wide-angle multi-element Hypergon micro-objective, composed of aspherical lenses smaller than 1 mm, which exhibits distortion-free imaging performance. The objective is fabricated by a multi-step femtosecond two-photon lithography process. To realize the design, we apply a novel (to the best of our knowledge) approach using shadow evaporation to create highly non-transparent aperture stops, which are crucial components in many optical systems. We achieve a field-of-view (FOV) of 70°, at a resolution of 12.4 μm, and distortion-free imaging over the entire FOV. In the future, such objectives can be directly printed onto complementary metal-oxide-semiconductor (CMOS) imaging chips to produce extremely compact, high-quality image sensors to yield integrated sensor devices used in industry. © 2020 Optical Society of America**

<https://doi.org/10.1364/OL.392253>

Compact non-distortive wide-angle objectives are highly desirable in state-of-the-art technologies, such as robotics or self-driving cars. However, the fabrication of such optics via classical manufacturing processes remains challenging and expensive. In recent years, femtosecond two-photon 3D printing has emerged as the technique of choice to produce high-performance imaging optics at a very small scale ( $<500\ \mu\text{m}$ ) [1–9]. This versatile manufacturing approach has been shown to be a highly promising tool for both the fabrication of single micro-optical components such as lenses [10–12], phase plates [13–19], or waveguides [20–24], as well as complex micro-optical systems, such as multi-lens objectives [1,4,13] or even entire scanning-probe microscopes [25]. Since it is an additive manufacturing process, 3D printing enables the straightforward fabrication of free-form surfaces [26–30], giving it a tremendous advantage over classical lens grinding methods. So far, one drawback of 3D printed imaging optics is that their material is limited to transparent ultraviolet (UV) curable photoresists. The lack of light-blocking features, such as lens tubes or apertures, inevitably leads to a loss of imaging quality. For example, wide-angle

objectives (objective lenses with an angular FOV of at least 55°) produce substantial geometric image distortion, unless it is specifically corrected for in the optical design. To do so, the integration of an absorptive aperture stop between two lens elements is essential [31]. Recently, Toulouse *et al.* have presented a method to create non-transparent components in micro-optics, based on superfine inkjet printing [32]. While this is a very promising approach toward more complex micro-optical systems, apertures created by this technique cannot be realized in every optical design, as they require enough space to integrate the ink mold. Additionally, precise control of the ink film thickness is challenging, and as a result, structures created this way are typically still slightly transparent. In this work, we propose a novel method to create thinner, completely non-transparent aperture stops based on shadow evaporation. With this fabrication method, we build a multi-element 3D printed wide-angle micro-objective that is offering nearly distortion-free imaging performance.

We use the ultra-wide-angle objective Hypergon (Optische Anstalt C. P. Goerz) [33] as a basis for our wide-angle micro-objective design. This photographic objective is composed of two strongly curved meniscus lenses, which are symmetrically arranged around an aperture. It is specifically designed to yield an astigmatically corrected and distortion-free image over a large FOV (135°). To make the design suitable for 3D printing, several adaptations have to be made. Most notably, the curvature of the two meniscus lenses must be reduced substantially to avoid them from sagging during or after the printing process. The spacing between components has to be increased to ensure that unexposed, liquid photoresist can be washed out and that the shape accuracy of the optical surfaces does not suffer due to the proximity effect [34]. In addition, the optical properties of the lens material have to be adjusted to those of the utilized photoresist IP-S ( $n_{588\ \text{nm}} = 1.5067$ ,  $\nu_d = 46.16$ ) [35]. Finally, since 3D printing techniques can produce them without any additional cost, we use aspheric surfaces in our simulations to correct spherical aberrations. In the original design, these were neglected in favor of correcting astigmatism and image distortion, while maintaining the large FOV; moreover, at that time,

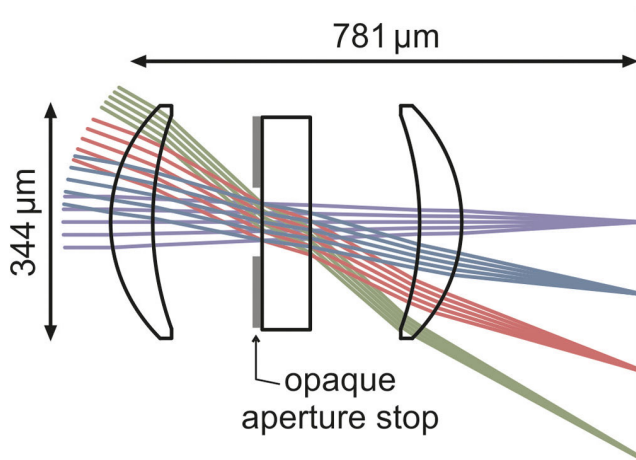


**Fig. 1.** Optical design of a wide-angle (FOV 60°) multi-lens Hypergon micro-objective suitable for 3D printing, acquired from sequential ray tracing with an effective focal length (distance from rear principal plane to imaging plane) of 605  $\mu\text{m}$  and an  $f$ -number of 8.

manufacturing and testing of aspheres was not common. We use the optical design software ZEMAX to generate an aberration corrected, distortion free micro-objective design with a FOV of 60°, meeting all of the above requirements. In addition to the image distortion, coma, astigmatism, and spherical aberrations were corrected. This design, as depicted in Fig. 1, consists of lenses with a diameter of 344  $\mu\text{m}$  and creates an image at a distance of 781  $\mu\text{m}$  behind the front lens vertex ( $f = 605 \mu\text{m}$ ). The surface shapes of the lenses are exported to the computer-aided design (CAD) software SolidWorks, where supporting structures (shown in Fig. 2) are added to adjoin the different parts. Including these structures, the maximum diameter of the objective is 780  $\mu\text{m}$ , resulting in a total volume  $< 1 \text{ mm}^3$ .

The micro-objective is fabricated from IP-S photoresist onto a glass substrate via a multi-step femtosecond two-photon 3D printing process using a Photonic Professional GT (Nanoscribe GmbH) and a 25x/NA0.8 microscope objective in dip-in configuration. This machine uses a femtosecond ( $\approx 100 \text{ fs}$ )-pulsed laser beam ( $\lambda = 780 \text{ nm}$ ) at a repetition rate of 80 MHz. The beam is scanned in the  $XY$  direction by galvanometric mirrors at a scanning speed of 50,000  $\mu\text{m/s}$ . More details on the fabrication technique can be found in the method section of [1]. The total writing time for a full wide-angle micro-objective is about 7 h. The entire fabrication process is illustrated in Fig. 2. In the first step, the bottom lens and a circular plate that will later serve as the aperture stop are printed [see Fig. 2(a)]. The top of the plate has a small sacrificial cap corresponding to the transparent part of the aperture attached to it. This cap can be removed with the aid of the predetermined breaking points highlighted in Fig. 2(a). Cross-shaped alignment markers are also added to the top of the plate. After development, a 200-nm-thick layer of silver (Ag) is deposited on top of the structure using e-gun evaporation [Fig. 2(b)]. As it is shadowed by the small cap, the inner part of the plate remains free of Ag and thus transparent. We then remove the cap to create the aperture stop, as illustrated in Fig. 2(c). This is done by carefully shearing it off with a thin needle, mounted onto a manual  $x,y,z$ -stage under a microscope. Afterwards, the top lens of the objective is printed directly onto the Ag film using the cross-shaped markers for alignment [Fig. 2(d)].

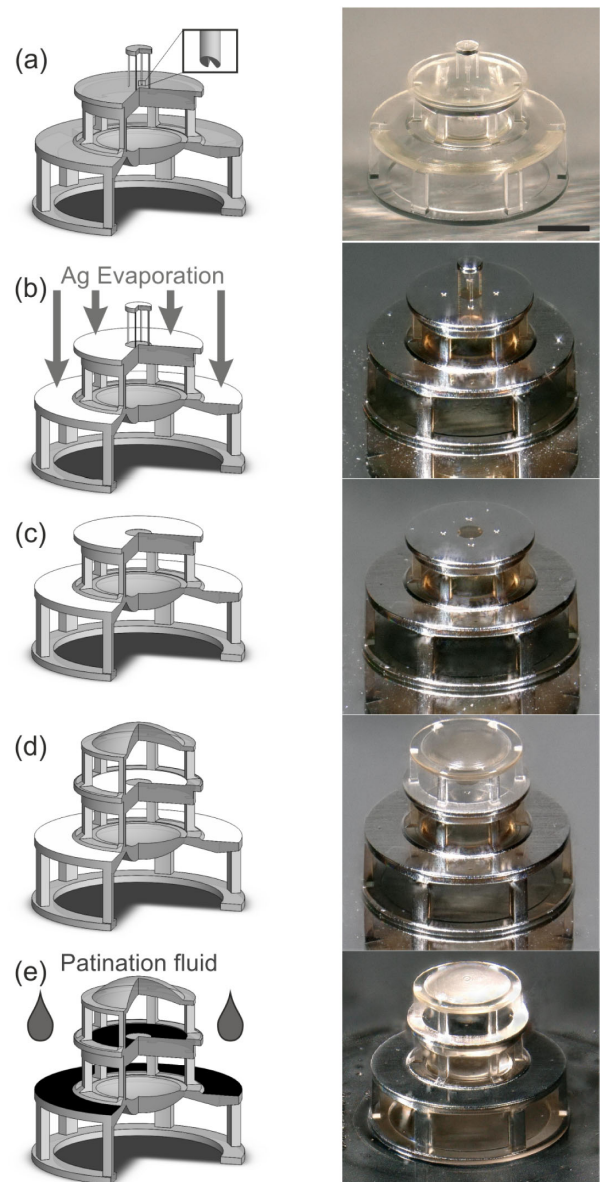


**Fig. 2.** Fabrication process of a multi-element wide-angle Hypergon micro-objective illustrated by CAD models (left) and microscope images (right). (a) The bottom part of the objective containing the first lens and a circular plate with a removable cap is 3D printed. The inset shows predetermined breaking points of the cap. Scale bar: 200  $\mu\text{m}$ . (b) A 200-nm-thick Ag film is evaporated on top. Since the removable cap shadows part of the circular plate, this creates a metal aperture stop. (c) The cap is removed at its predetermined breaking points. (d) The top part of the objective containing the second lens is 3D printed onto the aperture plate. (e) The Ag film is chemically oxidized using a patination fluid to reduce its reflectivity.

To decrease the high reflectivity of the aperture, which might lead to undesired stray light and ghost images, we oxidize the Ag using a commercially available patination fluid (Pariser Oxid Edloxid, Horst zu Jeddelloh GmbH), as depicted in Fig. 2(e). Patination is a process during which a metallic object develops a thin layer of oxidized metal on its surface. In the case of Ag, a layer of silver sulfide ( $\text{Ag}_2\text{S}$ ), which has a dark gray to black

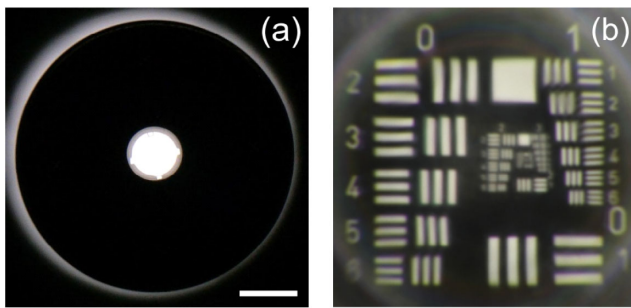


**Fig. 3.** (a) Microscope image of oxidized aperture taken with transmission illumination, indicating its precise positioning and high opacity. Scale bar: 100  $\mu\text{m}$ . (b) Image of a USAF 1951 resolution test target in the imaging plane of the wide-angle objective.

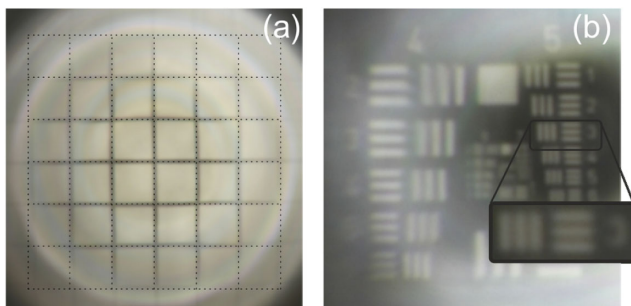


**Fig. 4.** Image of a rectangular grid with an undistorted grid superimposed as dashed lines. Lateral image distortion is less than 1%. (b) Groups 4, 5, 6, and 7 of the USAF 1951 resolution test target. The inset depicts that elements 3 of group 5 are still resolvable, which is equivalent to a resolution of 12.4  $\mu\text{m}$ .

appearance [see Fig. 2(e)] and a significantly reduced reflectivity ( $\approx 30\%$ ) [36] in the visible spectral range compared to Ag ( $\approx 98\%$ ) [37] can be formed. The patination fluid is diluted with ethanol (99.9%, Sigma-Aldrich) at a 1:3 ratio (patination fluid : ethanol) and drop-coated onto the micro-objective with a manual pipette, where it is left for 40 s. Dilution is necessary as using the pure fluid results in damage of the Ag film, rendering it partially transparent even after very short application times of just a few seconds. Afterwards, the sample is thoroughly flushed with ethanol to stop the reaction and wash off any left-over patination fluid from the micro-objective. The oxidized aperture stop (without the lens printed on top for better illustration) is shown in Fig. 3(a). Transmission illumination is used in this image to highlight the large optical contrast between the transparent and the non-transparent parts of the aperture. This demonstrates that when using our patination method, the opacity of the Ag film is not compromised.

To characterize the imaging properties of our micro-objective, images are recorded with a Nikon DS-Ri2 camera through a  $20\times$  (NA = 0.45) microscope objective using white light transmission illumination from a halogen lamp. Figure 3(b) displays the performance of the finished wide-angle micro-objective by imaging a USAF 1951 test target chart. The image exhibits a high optical contrast that cannot be achieved with conventional, all-transparent 3D-printed micro-optics. From this image, we determine the FOV of the objective to be

$70^\circ$ , even exceeding the designed  $60^\circ$ . To quantify the distortion, we replace the USAF 1951 test chart with a rectangular grid and record its depicted image at a distance of 50 mm. By relating the actual distance from the center of the image to the four outer corners of the imaged grid (AD) with the predicted distance of the undistorted grid (PD), we calculate a maximum image distortion ( $\% \text{distortion} = \frac{AD-PD}{PD} * 100\%$ ) of  $\approx 1\%$ , which is practically considered to be distortion-free imaging [31]. Finally, the USAF 1951 test chart is imaged again at a very short distance (2 mm) to assess the maximum resolution of the objective. As one can see in Fig. 4(b), the horizontal and vertical bars in element 3 of group 5 of the test chart are still clearly visible, corresponding to a resolution of 40.3 lp/mm or 12.4  $\mu\text{m}$ . We should mention here that it was possible to fabricate a similar design with  $60^\circ$  FOV and an image distortion of about 3%, which gave a resolution of about 4  $\mu\text{m}$ .

In conclusion, we successfully fabricated a complex wide-angle (FOV  $70^\circ$ ) micro-objective, exhibiting a high-imaging contrast and distortion-free imaging performance ( $\approx 1\%$ ) with a resolution of 12.4  $\mu\text{m}$  by using femtosecond 3D laser printing. To produce this design, we implemented, to the best of our knowledge, a novel approach to fabricate highly non-transparent apertures in 3D-printed micro-optical systems, based on Ag shadow evaporation. We demonstrated that the obtained Ag film could be oxidized using a commercially available patination fluid to yield a less reflective layer that serves well as an aperture stop. In the future, such high-performing wide-angle micro-objectives can be used to produce ultra-compact, highly integrated image sensors for industry applications.

**Funding.** Bundesministerium für Bildung und Forschung (13N14097, PRINOPTICS, PRINTFUNCTION, QLinkX); European Research Council (AdG COMPLEXPLAS, PoC 3DPRINTEDOPTICS); Baden-Württemberg Stiftung (Opterial).

**Disclosures.** The authors declare no conflicts of interest.

<sup>†</sup>These authors contributed equally to this work.

## REFERENCES

1. T. Gissibl, S. Thiele, A. Herkommer, and H. Giessen, *Nat. Photonics* **10**, 554 (2016).
2. S. Fischbach, A. Schlehahn, A. Thoma, N. Srocka, T. Gissibl, S. Ristok, S. Thiele, A. Kaganskiy, A. Strittmatter, T. Heindel, S. Rodt, A. Herkommer, H. Giessen, and S. Reitzenstein, *ACS Photon.* **4**, 1327 (2017).
3. S. Thiele, K. Arzenbacher, T. Gissibl, H. Giessen, and A. M. Herkommer, *Sci. Adv.* **3**, e1602655 (2017).
4. S. Thiele, C. Pruss, A. M. Herkommer, and H. Giessen, *Opt. Express* **27**, 35621 (2019).
5. S. Bianchi, V. P. Rajamanickam, L. Ferrara, E. Di Fabrizio, C. Liberale, and R. Di Leonardo, *Opt. Lett.* **38**, 4935 (2013).
6. H. Fan, X.-W. Cao, L. Wang, Z.-Z. Li, Q.-D. Chen, S. Juodkazis, and H.-B. Sun, *Opt. Lett.* **44**, 5149 (2019).
7. Z. Ma, X. Hu, Y. Zhang, X. Liu, Z. Hou, L. Niu, L. Zhu, B. Han, Q. Chen, and H.-B. Sun, *Adv. Funct. Mater.* **29**, 1903340 (2019).
8. J. Fischer and M. Wegener, *Laser Photon. Rev.* **7**, 22 (2013).
9. J. K. Hohmann, M. Renner, E. H. Waller, and G. von Freymann, *Adv. Opt. Mater.* **3**, 1488 (2015).
10. R. Guo, S. Xiao, X. Zhai, J. Li, A. Xia, and W. Huang, *Opt. Express* **14**, 810 (2006).
11. Z. Hong and R. Liang, *Sci. Rep.* **7**, 7145 (2017).

12. M. Schmid, S. Thiele, A. Herkommer, and H. Giessen, *Opt. Lett.* **43**, 5837 (2018).
13. A. Žukauskas, M. Malinauskas, and E. Brasselet, *Appl. Phys. Lett.* **103**, 181122 (2013).
14. K. Weber, F. Hütt, S. Thiele, T. Gissibl, A. Herkommer, and H. Giessen, *Opt. Express* **25**, 19672 (2017).
15. T. Gissibl, M. Schmid, and H. Giessen, *Optica* **3**, 448 (2016).
16. Q.-D. Chen, D. Wu, L.-G. Niu, J. Wang, X.-F. Lin, H. Xia, and H.-B. Sun, *Appl. Phys. Lett.* **91**, 171105 (2007).
17. E. Brasselet, M. Malinauskas, A. Žukauskas, and S. Juodkazis, *Appl. Phys. Lett.* **97**, 211108 (2010).
18. E. Stegenburgs, A. Bertocini, A. Trichili, M. S. Alias, T. K. Ng, M. Alouini, C. Liberale, and B. S. Ooi, *IEEE Commun. Mag.* **57**(8), 65 (2019).
19. V. Hahn, P. Kiefer, T. Frenzel, J. Qu, E. Blasco, C. Barner-Kowollik, and M. Wegener, *Adv. Funct. Mater.* 1907795 (2020).
20. P.-I. Dietrich, M. Blaicher, I. Reuter, M. Billah, T. Hoose, A. Hofmann, C. Caer, R. Dangel, B. Offrein, U. Troppenz, M. Moehle, W. Freude, and C. Koos, *Nat. Photonics* **12**, 241 (2018).
21. A. Nestic, M. Blaicher, T. Hoose, A. Hofmann, M. Lauermann, Y. Kutuvantavida, M. Nöllenburg, S. Randel, W. Freude, and C. Koos, *Opt. Express* **27**, 17402 (2019).
22. A. Landowski, D. Zepp, S. Wingerter, G. von Freymann, and A. Widera, *APL Photon.* **2**, 106102 (2017).
23. G. Panusa, Y. Pu, J. Wang, C. Moser, and D. Psaltis, *Opt. Mater. Express* **9**, 128 (2019).
24. Q. Shi, B. Sontheimer, N. Nikolay, A. W. Schell, J. Fischer, A. Naber, O. Benson, and M. Wegener, *Sci. Rep.* **6**, 31135 (2016).
25. P. Dietrich, G. Göring, M. Trappen, M. Blaicher, W. Freude, T. Schimmel, H. Hölscher, and C. Koos, *Small* **16**, 1904695 (2020).
26. C. Liberale, G. Cojoc, P. Candeloro, G. Das, F. Gentile, F. De Angelis, and E. Di Fabrizio, *IEEE Photon. Technol. Lett.* **22**, 474 (2010).
27. T. Gissibl, S. Thiele, A. Herkommer, and H. Giessen, *Nat. Commun.* **7**, 11763 (2016).
28. H. E. Williams, D. J. Freppon, S. M. Kuebler, R. C. Rumpf, and M. A. Melino, *Opt. Express* **19**, 22910 (2011).
29. L. Jonušauskas, D. Gailevičius, L. Mikoliūnaitė, D. Sakalauskas, S. Šakirzanovas, S. Juodkazis, and M. Malinauskas, *Materials (Basel)* **10**, 12 (2017).
30. D. Loterie, P. Delrot, and C. Moser, *Nat. Commun.* **11**, 852 (2020).
31. R. E. Fischer, B. Tadic-Galeb, and P. R. Yoder, *Optical System Design*, 2nd ed. (McGraw-Hill, 2008).
32. A. Toulouse, S. Thiele, H. Giessen, and A. M. Herkommer, *Opt. Lett.* **43**, 5283 (2018).
33. C. P. Goerz, "Astigmatically-corrected wide-angle objective," U.S. patent 3,555,200A (12 August 1900).
34. E. H. Waller and G. Von Freymann, *Polymers (Basel)* **8**, 297 (2016).
35. T. Gissibl, S. Wagner, J. Sykora, M. Schmid, and H. Giessen, *Opt. Mater. Express* **7**, 2293 (2017).
36. D. P. Adams, R. S. Goeke, C. E. Sobczak, E. D. Jones, and M. A. Rodriguez, *Metal Sulfide Thin Films* (2012).
37. E. Fearon, T. Sato, D. Wellburn, K. Watkins, and G. Dearden, in *Proceedings of the International Conference Laser Assisted Net Shape Engineering* (2007), p. 5.